ACS APPLIED MATERIALS & INTERFACES

Research Article

www.acsami.org

Synthesis of Hierarchical Iron Hydrogen Phosphate Crystal as a Robust Peroxidase Mimic for Stable H_2O_2 Detection

Tongbao Zhang, Yangcheng Lu,* and Guangsheng Luo

Department of Chemical Engineering, State Key Laboratory of Chemical Engineering, Tsinghua University, Beijing 100084, China

Supporting Information

ABSTRACT: To develop a green, cost-efficient and robust peroxidase mimic, micro/nano hierarchical morphology (for ease of separation and reuse), relative chemically stable composition (for ease of storage) and stable crystal structure (for long-term stability) are highly desired. Herein, using phosphoric acid as a chelating ligand to control the release of iron ions, hierarchical iron(III) hydrogen phosphate hydrate crystals are successfully prepared by nanosheets formation and following self-assembling in a facile low-temperature hydrothermal process. They are first found to have peroxidase-like activity and showed higher affinity for H_2O_2 and lower affinity for 3,3′,5,5′-tetramethylbenzidine compared with horseradish peroxidase. The affinity feature is used for quantitative detection of H_2O_2 and shows a wide linear detection range from 57.4 to 525.8 μM (R^2 = 0.994) with a low detection limit of 1 μM. Benefited from chemical stability of hierarchical iron(III) salt crystals, they own good reproducibility (relative standard deviation = 1.95% for 10 independent measurements), long-term stability (no activity loss after 10 cycles), and ease of recovery (by simple centrifugation). Because the method is easily accessible, iron hydrogen phosphate hierarchical crystals have great potential for practical use of H_2O_2 sensing and detection under harsh conditions.

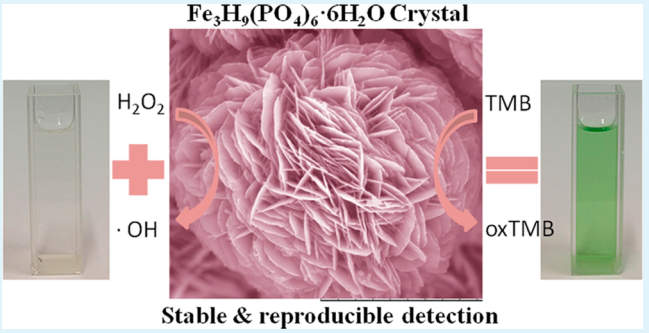

KEYWORDS: *hierarchical morphology, iron(III) hydrogen phosphate crystals, peroxidase mimic, H_2O_2 detection, hydrothermal process*

INTRODUCTION

Peroxidases are ubiquitous in nature and are generally proteins with high efficiency and specificity under mild conditions.[1] They show significance in analytical diagnostics, such as H_2O_2, glucose, and melamine detection.[2−4] However, their drawbacks[5−7] have gradually emerged in practical applications and include (1) lack of stability and loss of activation in harsh conditions and (2) cost and time-consuming preparation and purification. Artificial enzyme mimics are becoming a research interest because of their remarkable superiorities over traditional organic enzymes for ease of preparation, low price, and good stability in activity.

Inorganic materials have long been misunderstood to be biologically inert and customarily used as supports for enzymes in organic/inorganic hybrids. Since Gao et al.[8] reported intrinsic peroxidase-like activity of Fe_3O_4 nanoparticles similar to that of horseradish peroxidase (HRP), the field for the development of inorganic materials as peroxidase mimics has subsequently opened. A variety of inorganic materials were investigated and discovered to possess similar activities, such as CeO_2,[9] Co_3O_4,[10] MFe_2O_4 (M = Co, Mn, Zn),[11−13] CuO,[14] MnO_2,[15] Au,[16] Pt[17] nanoparticles, carbon-based nanomaterials[18] (fullerene, carbon nantubes, and graphene), etc.[19−21] These reported materials are commonly nanoparticles taking advantage of large surface-to-volume ratios for effective interaction with substrates. However, their inherent disadvantageous limitations are also obvious. For example, most nanoparticles are used in a disposable way. Because they are always notable/heavy metals or notable/heavy metals-containing compounds, the disposable way of usage causes two main problems. One is the loss of notable metals, which brings economic concerns; the other is the toxicity and pollution caused by the wasted heavy metal contained mimics.[22] These limitations make nanoparticles not be green and cost-efficient peroxidise mimics. Besides, the uncontrolled proneness of nanomaterials aggregation weakens the reproducibility and reliability of the analytical results, which is significantly important for detection usage.[23]

Thus, to develop a peroxidase mimic, stable micro/nano stereostructures are highly desirable to overcome the above-mentioned limitations. On the one hand, the primary nanostructure provides a large surface area to interact with substrates; on the other hand, the secondary microstructure makes them easy to separate and reuse. As they are recovered for reuse, the stability of the structure must be taken into consideration. Crystals with regular structure are good

Received: June 12, 2014
Accepted: July 16, 2014
Published: July 16, 2014

   dx.doi.org/10.1021/am503708a | ACS Appl. Mater. Interfaces 2014, 6, 14433−14438

candidates. Except for stability, some work also confirms the activity of the mimics is strongly dependent on crystallinity and structure.[24] For example, the peroxidase-like activities of Fe_3O_4 nanocrystals were the following: the order of cluster spheres > triangular plates > octahedral, in which the exposure of surface facets like {220}, {100}, and {111} of octahedral would enhance its catalytic activity;[25,26] sheet-like FeS and well-defined CuS concave polyhedral superstructures have more sensitive response than spherical ones as H_2O_2 sensors.[27,28] The results emphasize that the development of new stereo-structural peroxidase mimics with a specific crystalline structure is urgently necessary and important. Until now, the reports are still few with respect to the stability and reproducibility of catalysis performance.

Iron phosphate compounds are a large family of inorganic materials with good catalytic activity and biocompatibility, and could be endowed with varieties of stereostructures and crystalline structures.[29,30] Crystalline iron phosphates have high stability, even under hydrothermal conditions with the existence of strong acids. Considering the specific electron-transfer ability is the common requirement of these iron phosphate catalysts and natural peroxidases,[31,32] iron phosphate crystals are potential robust peroxidase mimics. Herein, we fabricated iron hydrogen phosphate crystals (FeHPO) with hierarchical morphology and first demonstrated their peroxidase-like activity of such pure iron(III) salt crystals (Supporting Information, Figure S1) for the detection of H_2O_2. They show a wide H_2O_2 detection range (57.4 to 525.8 μM) with a low detection limit (1 μM). Besides, benefited from the micro/nano hierarchical morphology, they are easy to separate and reuse, making them a green and cost-efficient peroxidase mimic. The pure iron(III) salt composition also makes them extremely easy to store. To the best of our knowledge, the good reproducibility and long-term stability performance benefited from the specific crystal structure is also first reported, which is of great importance for bio/chemical detection.

RESULTS AND DISCUSSIONS

The general morphologies of the prepared product were observed by scanning electron microscopy (SEM), and the results are illustrated in Figure 1a–d. The prepared material is uniform in all observation fields and presents hierarchical micro/nano structures with flower-shaped morphologies (Figure 1a,b). The statistical analysis yielded an average size of a single hierarchical structure as ca. 13 ± 2 μm. Further investigation on a flower-shaped microsphere declares the hierarchical structure is composed of ultrathin nanosheets intermingled with each other in very high density. The surface of the nanosheets is smooth and the average thickness of them is ca. 10 ± 3 nm (Figure 1c,d).

The information on the phase purity and crystal structure of the products was investigated by the high-precision scanning powder X-ray diffraction technique. The diffraction data (black line in Figure 2) collected on the powder diffraction beamline (D8 Advance) at a wavelength λ = 1.540 56 Å indicated a phase of iron hydrogen phosphate hydrate ($Fe_3H_9(PO_4)_6{\cdot}6H_2O$; PDF #44-0812) was obtained. Meanwhile, minor impurities with a diffraction peak at 20.3° corresponded to iron phosphate hydrate ($FePO_4{\cdot}2H_2O$; PDF #15-0513) were also detected. The phase purity of $Fe_3H_9(PO_4)_6{\cdot}6H_2O$ is 92.64 wt % calculated by the full spectrum fitting method. To further promulgate the crystal structure of the iron hydrogen

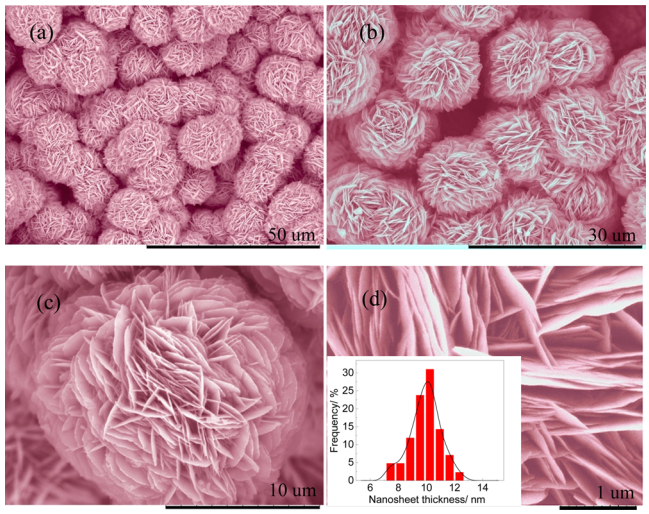

Figure 1. Scanning electron microscope images of as-prepared products. From (a) to (d), it corresponds to various magnification. The inset of panel d presents the distribution of nanosheet thickness.

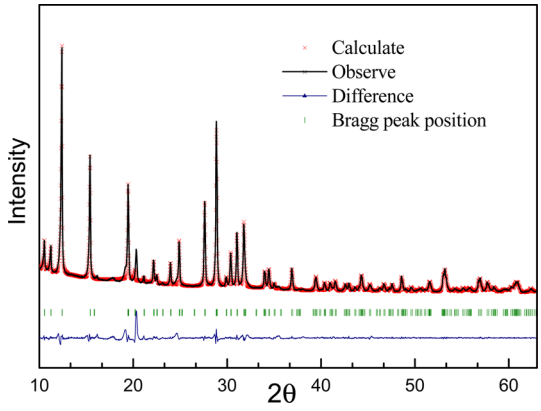

Figure 2. Final Rietveld-refined fit to the XRD data (λ = 1.540 56 Å) for iron hydrogen phosphate hydrate $Fe_3H_9(PO_4)_6{\cdot}6H_2O$. The experimental data (black line), calculated pattern (red dots), and the difference curve (lower blue line) are shown. Vertical lines indicate the Bragg peak positions for $Fe_3H_9(PO_4)_6{\cdot}6H_2O$ (olive lines).

phosphate, all the diffraction peaks were indexed and finally refined to the hexagonal structure (space group = $P3$, No. 143) with lattice parameters $a = b$ = 9.1379 Å, c = 16.8475 Å, $\alpha = \beta$ = 90°, and γ = 120°. The Rietveld-refinement of a hexagonal structure model against observed XRD data led to the fit shown in Figure 2. The refinement results were well fitted to the observed XRD data with a low residual error of R_{wp} = 6.84% and R_p = 3.69%.

The possible mechanism for the synthesis of hierarchical iron hydrogen phosphate was investigated and concluded as the bottom-up self-assembly process. First, dispersed small nanosheets would be generated under the specific hydrothermal condition. Due to the relatively strong coordinating ability, phosphates would coordinate with iron ions (Fe^{3+}) to form stable ionic structures. Theoretical calculation on the iron species at various pH values is plotted in Figure 3a. The results revealed that under pH = 1.12 of the initial reaction system, iron species basically coordinates with $H_2PO_4^-$ and HPO_4^{2-}, and exists in a formula of $[FeH_2PO_4]^+$ (95.2%) and $[FeHPO_4]^{2+}$ (4.3%). The formation of the complex can sharply reduce the availability of free Fe^{3+} in aqueous solution and thus

dx.doi.org/10.1021/am503708a | ACS Appl. Mater. Interfaces 2014, 6, 14433–14438

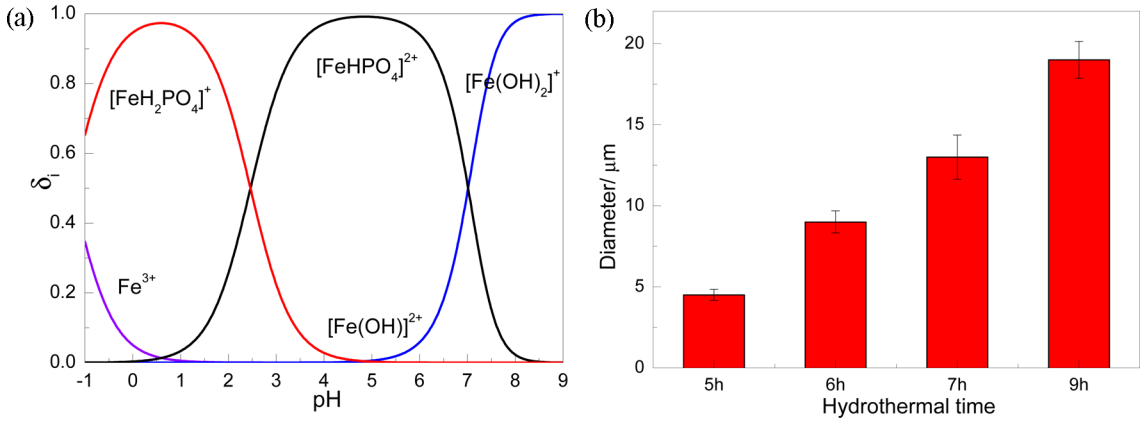

Figure 3. (a) Calculated distribution results of iron species at various pH values. (b) Statistical average diameter of samples observed after different periods of hydrothermal treatment.

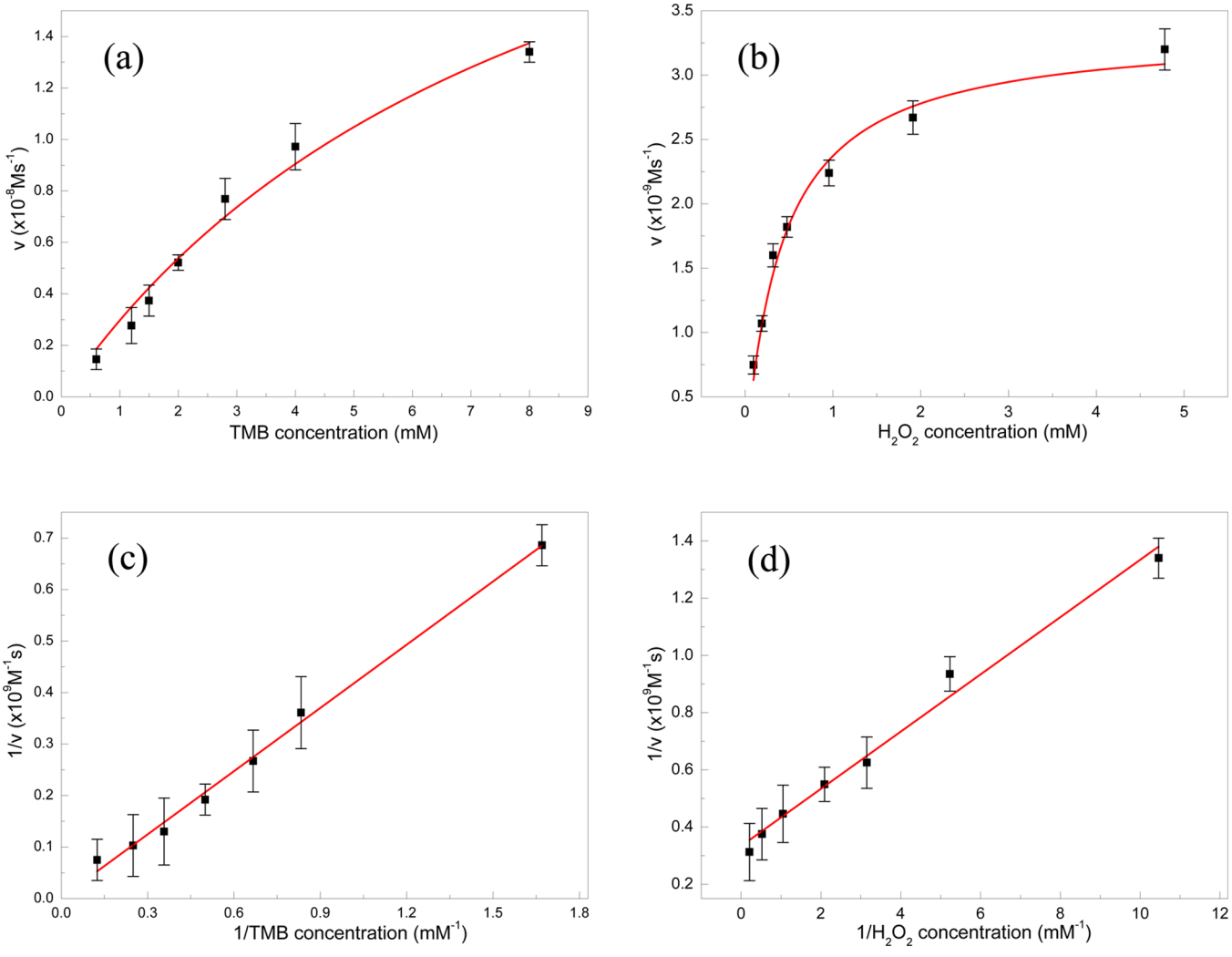

Figure 4. Steady-state kinetic analysis using the Michaelis–Menten model (a, b) and Lineweaver–Burk model (c, d) for hierarchical FeHPO. The concentration of H_2O_2 was 0.478 mM and TMB concentration was varied (a, c). The concentration of TMB was 1 mM and H_2O_2 concentration was varied (b, d).

leads to a low precipitation rate, which was critical for the formation of nanosheets morphology. A comparison experiment was also conducted to verify the rationality of our proposed mechanism by using noncoordinated nitric acid to replace phosphoric acid, in which the product obtained was composed of irregular particles and bulks due to lack of controlled release of Fe^{3+} (Supporting Information, Figure S3). Second, self-assembly of nanosheets would spontaneously happen, driven by the minimum energy principle, leading to the formation of micro/nano hierarchical structure. The

dx.doi.org/10.1021/am503708a | ACS Appl. Mater. Interfaces 2014, 6, 14433−14438

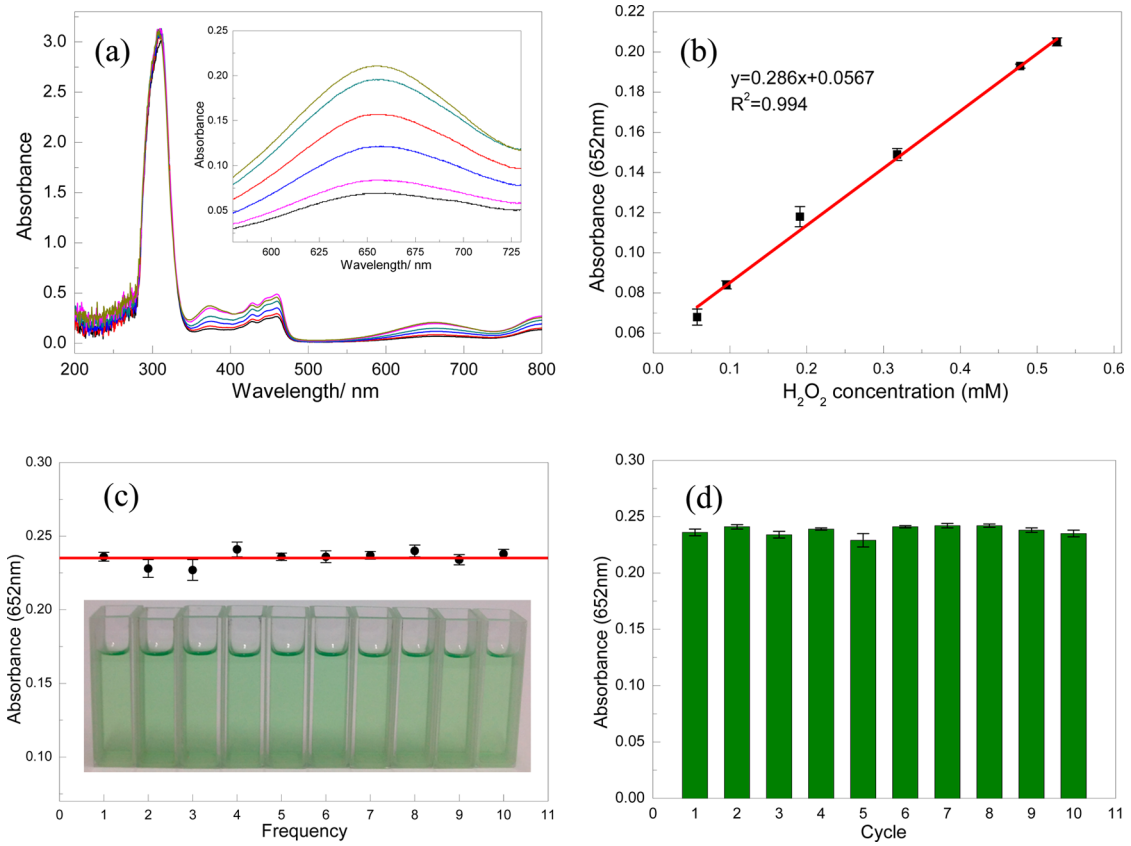

Figure 5. (a) Typical UV−vis spectra of reaction system at 1 mM TMB varied H_2O_2 concentrations, from bottom to top, corresponds to 57.4, 95.6, 191.2, 317.8, 478, and 525.8 μM. (b) Linear fitting plot between the absorbance at 652 nm against concentration of H_2O_2. (c) Reproducibility experiments and corresponding color change of each independent experiment. (d) Stability experiments conducted at FeHPO 0.478 and H_2O_2 1.1 mM TMB conditions.

primary nanosheets would continue to grow until the depletion of the iron source. Accordingly, the micro/nano structure would be well-developed (Supporting Information, Figure S2) and the average size of the assemblies would continuously grow (Figure 3b). However, if hydrothermal treatment was over extended, the density of the nanosheets might be so high that the surfaces with high energy would be easily agglomerated (Supporting Information, Figure S 2d).

The peroxidase-like activity of the hierarchical FeHPO was evaluated through the catalysis of a colorless peroxidase substrate, 3,3′,5,5′-tetramethylbenzidine (TMB), in the presence of H_2O_2 to generate a colorimetric reaction. The inset of Figure S4 (Supporting Information) clearly illustrates the hierarchical FeHPO could catalyze the oxidation of TMB substrate with H_2O_2, and produced a nice green color. The color change is different from the blue color elsewhere. It might be because TMB was dissolved in absolute alcohol in our work, different from dimethylformamide (DMF) or other solvents. In contrast, the reaction systems of FeHPO−H_2O_2, FeHPO−TMB, and H_2O_2−TMB did not present any perceptible color change. The colorimetric reaction could also be monitored spectrophotometrically from absorbance augmentation of TMB oxidation products at 652 nm. The UV−vis spectra (Supporting Information, Figure S4) also confirm the color change phenomenon and show a significant increase of absorbance at 652 nm compared with control groups. These results clearly confirmed intrinsic peroxidase-like activity of as-prepared FeHPO hierarchical crystals.

Similar to other peroxidase mimics, the activity of FeHPO crystals are affected by temperature and pH conditions as well. The results are shown in Figure S5 (Supporting Information). Herein, pH = 3 and T = 80 °C are optimum conditions for FeHPO crystals and are adopted as the standard conditions for the following investigation.

The peroxidase-like activity of the hierarchical FeHPO was further investigated by steady-state kinetic experiments (Supporting Information, Figure S6). Over a suitable range of TMB and H_2O_2 concentrations, the plots of initial reaction rates vs TMB or H_2O_2 concentration show typical Michaelis−Menten behavior (Figure 4a,b). By plotting reaction rate against substrate concentration, the catalytic parameters, K_m and v_{max}, were determined using the Michaelis−Menten model. The K_m value of hierarchical FeHPO with H_2O_2 as substrate was 0.41 mM, which was much lower than the reported value for horseradish peroxidase (HRP, 3.7 mM). However, the K_m value of hierarchical FeHPO with TMB as the substrate was 8.63 mM, which was higher than that of HRP (0.434 mM). All of the parameters were also regressed to the Lineweaver−Burk double-reciprocal model ($1/v_0$ vs $1/[S]$), which also gave the analogous values (Figure 4c,d). The K_m value characterizes affinity of substrates to enzymes. And the lower value means the higher affinity. The results indicate that hierarchical FeHPO has a lower affinity for TMB than HRP, corresponding to a relative higher TMB concentration used in experiments. However, it has a much higher affinity for H_2O_2, which may be due to the fact that a HRP molecular has only one iron ion, in contrast to the surface of FeHPO hierarchical structures.

Besides, the unique stereomorphology and specific crystal structure might also benefit for the reaction performance. A higher affinity for H_2O_2 would accelerate the generation of HO· and HO_2· and catalyze the oxidation of TMB (Supporting Information, eq S1). The lower affinity for TMB could also guarantee maximum active sites would be available for H_2O_2. The affinity feature of hierarchical FeHPO for H_2O_2 and TMB would be advantageous to the colorimetric detection of H_2O_2.

The color variation caused by TMB oxidation was dependent on H_2O_2 concentration and can be monitored by absorbance change at 652 nm. The phenomenon could be used as a strategy for quantitative detection of H_2O_2. Figure 5a presents the UV−vis spectra monitoring the reaction system, which clearly shows an increase of absorbance at 652 nm. Figure 5b shows the calibration curve of the absorbance values against H_2O_2 concentration. The curve was linear in the range from 57.4 to 525.8 μM. The linear regression equation was $y = 0.286x + 0.0567$ (x: mM, $R^2 = 0.994$). To determine the detection limit of H_2O_2, blank samples were measured at 652 nm for 13 times (Supporting Information, Figure S7a). Blank samples here were 25 mg/mL FeHPO and 1 mM TMB. And the reactions were conducted at optimized conditions of $T = 80$ °C, pH = 3. Triple fluctuation of the baseline ($S/N = 3$) was determined to be the detection limit. When the H_2O_2 concentration in the FeHPO−H_2O_2−TMB reaction system was gradually decreased, the absorbance gradually decreased (Supporting Information, Figure S7b). When H_2O_2 concentration was below 1 μM, the absorbance was located in the triple fluctuation range of the baseline. Thus, the detection limit of the method was determined to be 1 μM.

The reproducibility of the method was investigated by conducting the experiment independently for 10 times. Figure 5c shows the measuring results of each experiment. The relative standard deviation (RSD) of these independent values was 1.95%, indicating good reproducibility of the method. The conclusion was also evidenced by nearly the same color change in each reaction system. Furthermore, as a crystal-based catalyst, two potential advantages are its stable activity and ease of recovery for reuse. Thus, FeHPO crystals were recycled by simple centrifugation and the peroxidase-like activity of each cycle was determined. Figure 5d presents the cycle performance of FeHPO crystals and Figure S7c (Supporting Information) shows the color change of each cycle. The results reveal no loss of activity was observed, even after 10 cycles. Besides, the RSD of the absorbance values is only 1.77%, indicating their good reproducibility, even when they were reused.

CONCLUSION

In conclusion, a facile method, based on the reaction of iron and phosphate ions with phosphoric acid as the chelating ligand for iron ions, was successfully developed for the preparation of hierarchical iron hydrogen phosphate hydrate crystals. Their peroxidase-like activity was first demonstrated. The steady-state kinetic analysis showed they have higher affinity for H_2O_2 and lower affinity for TMB compared with HRP. The affinity feature for H_2O_2 and TMB was further used for quantitative detection of H_2O_2 and showed a wide linear detection range from 57.4 to 525.8 μM ($R^2 = 0.994$) with a detection limit of 1 μM. The method showed good reproducibility with RSD = 1.95% for 10 independent measurements. Additionally, FeHPO peroxidase mimics had long-term stability (no activity loss after 10 cycles) and ease of recovery. Because the method is easily accessible, iron hydrogen phosphate hydrate hierarchical crystals have great potential for practical use in H_2O_2 sensing and detection under harsh conditions.

ASSOCIATED CONTENT

Supporting Information

Experiment details on the synthesis of hierarchical iron hydrogen phosphate hydrate crystals, evidence for pure iron(III) salt crystals, time dependent morphology evolution, evidence for confirming peroxidase-like activity, influence factors on peroxidase-like activity, steady-state kinetic measurements, possible mechanism of peroxidase-like activity for hierarchical FeHPO, and detection limit for H_2O_2. This material is available free of charge via the Internet at http://pubs.acs.org.

AUTHOR INFORMATION

Corresponding Author

*Y. Lu. Tel: +86 10 62773017. Fax: +86 10 62770304. E-mail: luyc@tsinghua.edu.cn.

Author Contributions

The paper was written through contributions of all authors. All authors have given approval of the final version of the paper.

Notes

The authors declare no competing financial interest.

ACKNOWLEDGMENTS

The authors are gratefully thankful for the support of the National Natural Science Foundation of China (20876084, 21036002, 21176136) and National Basic Research Program of China (2007CB714302) on this work.

REFERENCES

(1) Josephy, P. D.; Eling, T. R.; Mason, P. The Horseradish Peroxidase-Catalyzed Oxidation of 3,5,3′,5′-Tetramethylbenzidine. Free Radical and Charge-Transfer Complex Intermediates. *J. Biol. Chem.* **1982**, *257*, 3669−3675.

(2) Malvi, B.; Panda, C.; Dhar, B. B.; Gupta, S. S. One Pot Glucose Detection by [Fe^{III}(biuret-amide)] Immobilized on Mesoporous Silica Nanoparticles: An Efficient HRP Mimic. *Chem. Commun.* **2012**, *48*, 5289−5291.

(3) Song, Y. J.; Qu, K. G.; Zhao, C.; Ren, J. S.; Qu, X. G. Graphene Oxide: Intrinsic Peroxidase Catalytic Activity and Its Application to Glucose Detection. *Adv. Mater.* **2010**, *22*, 2206−2210.

(4) Wei, H.; Wang, E. Fe_3O_4 Magnetic Nanoparticles as Peroxidase Mimics and Their Applications in H_2O_2 and Glucose Detection. *Anal. Chem.* **2008**, *80*, 2250−2254.

(5) Song, Y. J.; Wang, X. H.; Zhao, C.; Qu, K. G.; Ren, J. S.; Qu, X. G. Label-free Colorimetric Detection of Single Nucleotide Polymorphism by Using Single-Walled Carbon Nanotube Intrinsic Peroxidase-like Activity. *Chem.—Eur. J.* **2010**, *16*, 3617−3621.

(6) Song, Y. J.; Qu, X. G. Colorimetric Biosensing Using Smart Material. *Adv. Mater.* **2011**, *23*, 4215−4236.

(7) Zhang, L.; Zhang, Q.; Li, J. H. Layered Titanate Nanosheets Intercalated with Myoglobin for Direct Electrochemistry. *Adv. Funct. Mater.* **2007**, *17*, 1958−1965.

(8) Gao, L. Z.; Zhuang, J.; Nie, L.; Zhang, J. B.; Zhang, Y.; Gu, N.; Wang, T. H.; Feng, J.; Yang, D. L.; Perrett, S.; Yan, X. Y. Intrinsic Peroxidase-like Activity of Ferromagnetic Nanoparticles. *Nat. Nanotechnol.* **2007**, *2*, 577−283.

(9) Celardo, I.; Pedersen, J. Z.; Traversa, E.; Ghibelli, L. Pharmacological Potential of Cerium Oxide Nanoaprticles. *Nanoscale* **2011**, *3*, 1411−1420.

(10) Mu, J. H.; Wang, Y.; Zhao, M.; Zhang, Li. Intrinsic Peroxidase-like Activity and Catalase-like Activity of Co_3O_4 Nanoparticles. *Chem. Commun.* **2012**, *48*, 2540−2542.

(11) Fan, Y. W.; Huang, Y. M. The Effective Peroxidase-like Activity of Chitosan-Functionalized $CoFe_2O_4$ Nanoparticles for Chemiluminescence Sensing of Hydrogen Peroxide and Glucose. *Analyst* **2012**, *137*, 1225−1231.
(12) Bhattacharya, D.; Baksi, A.; Banerjee, I.; Ananthakrishnan, R.; Maiti, T. K.; Pramanik, P. Development of Phosphate Modified $Fe_{(1-x)}MnxFe_2O_4$ Mixed Ferrite Nanoparticles: Novel Peroxidase Mimetics in Enzyme Linked Immunosorbent Assay. *Talanta* **2011**, *86*, 337−348.
(13) Su, L.; Feng, J.; Zhou, X. M.; Ren, C. L.; Li, H. H.; Chen, X. G. Colorimetric Detection of Urine Glucose Based $ZnFe_2O_4$ Magnetic Nanoparticles. *Anal. Chem.* **2012**, *84*, 5753−5758.
(14) Chen, W.; Chen, J.; Feng, Y. B.; Hong, L.; Chen, Q. Y.; Wu, L. F.; Lin, X. H.; Xia, X. H. Peroxidase-like Activity of Water-Soluble Cupric Oxide Nanoparticles and Its Analytical Application for Detection of Hydrogen Peroxide and Glucose. *Analyst* **2012**, *137*, 1706−1712.
(15) Wan, Y.; Qi, P.; Zhang, D.; Wu, J. J.; Wang, Y. Manganese Oxide Nanowire-Mediated Enzyme-Linked Immunosorbent Assay. *Biosens. Bioelectron.* **2012**, *33*, 67−74.
(16) Ju, Y.; Li, B. X.; Cao, R. Positively-Charged Gold Nanoparticles as Peroxidase Mimic and Their Application in Hydrogen Peroxide and Glucose Detection. *Chem. Commun.* **2010**, *46*, 8017−8019.
(17) Ma, M.; Zhang, Y.; Gu, N. Peroxidase-like Catalytic Activity of Cubic Pt Nanocrystals. *Colloids Surf., A* **2011**, *373*, 6−10.
(18) Liu, M.; Zhao, H. M.; Chen, S.; Yu, H. T.; Quan, X. Interface Engineering Catalytic Grapheme for Smart Colorimetric Biosensing. *ACS Nano* **2012**, *6*, 3142−3151.
(19) Liu, S.; Tian, J. Q.; Wang, L.; Luo, Y. L.; Chang, G. H.; Sun, X. P. Iron-Substituted SBA-15 Microparticles: A Peroxidase-like Catalyst for H_2O_2 Detection. *Analyst* **2011**, *136*, 4894−4897.
(20) Wang, Y. L.; Chen, S. H.; Ni, F.; Gao, F.; Li, M. G. Peroxidase-like Layered Double Hydroxide Nanoflakes for Electrocatalytic Reduction of H_2O_2. *Electroanalysis* **2009**, *21*, 2125−2132.
(21) Tian, J. Q.; Liu, S. Y.; Luo, L.; Sun, X. P. Fe(III)-based Coordination Polymer Nanoparticles: Peroxidase-like Catalytic Activity and Their Application to Hydrogen Peroxide and Glucose Detection. *Catal. Sci.Technol.* **2012**, *2*, 432−436.
(22) Baati, T.; Njim, L.; Neffati, F.; Kerkeni, A.; Bouttemi, M.; Gref, R.; Najjar, M. F.; Zakhama, A.; Couvreur, P.; Serre, C.; Horcajada, P. In Depth Analysis of the *in Vivo* Toxicity of Nanoparticles of Porous Iron(III) Metal−Organic Frameworks. *Chem. Sci.* **2013**, *4*, 1597−1607.
(23) Yang, H.; Zhang, X.; Tang, A.; Qiu, G. Cobalt Ferrite Nanoparticles Prepared by Coprecipitation/Mechanochemical Treatment. *Chem. Lett.* **2004**, *33*, 826.
(24) Nath, S.; Kaittanis, C.; Ramachandran, V.; Dalal, N. S.; Perez, J. M. Synthesis, Magnetic Characterization, and Sensing Applications of Novel Dextran-Coated Iron Oxide Nanorods. *Chem. Mater.* **2009**, *21*, 1761−1767.
(25) Liu, S. H.; Lu, F.; Xing, R. M.; Zhu, J. J. Structural Effects of Fe_3O_4 Nanocrystals on Peroxidase-like Activity. *Chem.—Eur. J.* **2011**, *17*, 620−625.
(26) Puvvada, N.; Panigrahi, P. K.; Mandal, D.; Pathak, A. Shape Dependent Peroxidase Mimetic Activity towards Oxidation of Pyrogallol by H_2O_2. *RSC Adv.* **2012**, *2*, 3270−3273.
(27) Dai, Z. H.; Liu, S. H.; Bao, J. C.; Ju, H. X. Nanostructured FeS as a Mimic Peroxidase for Biocatalysis and Biosensing. *Chem.—Eur. J.* **2009**, *15*, 4321−4326.
(28) He, W. W.; Jia, H. M.; Li, X. X.; Lei, Y.; Li, J.; Zhao, H. X.; Mi, L. W.; Zhang, L. Z.; Zheng, Z. Understanding the Formation of CuS Concave Superstructures with Peroxidase-like Activity. *Nanoscale* **2012**, *4*, 3501−3506.
(29) Zhang, T. B.; Lu, Y. C.; Luo, G. S. Iron Phosphate Prepared by Coupling Precipitation and Aging: Morphology, Crystal Structure, and Cr(III) Adsorption. *Cryst. Growth Des.* **2013**, *13*, 1099−1109.
(30) Zhang, T. B.; Lu, Y. C.; Luo, G. S. Synthesis of Single-Crystal Dendritic Iron Hydroxyl Phosphate as a Fenton Catalyst. *CrystEngComm* **2013**, *15*, 9104−9111.
(31) Jeong, M. S.; Jang, S. B. Electron Transfer and Nano-Scale Motions in Nitrogenase Fe-Protein. *Curr. Nanosci.* **2006**, *2*, 35−41.
(32) Markovic, Z.; Trajkovic, V. Biomedical Potential of the Reactive Oxygen Species Generation and Quenching by Fullerenes. *Biomaterials* **2008**, *29*, 3561−3573.